Search for B mesogenesis at *BABAR*

J. P. Lees, V. Poireau, V. Tisserand, E. Grauges, A. Palano, G. Eigen, D. N. Brown, Yu. G. Kolomensky, M. Fritsch, H. Koch, R. Cheaib, C. Hearty, T. S. Mattison, J. A. McKenna, R. Y. So, V. E. Blinov, A. R. Buzykaev, V. P. Druzhinin, E. A. Kozyrev, E. A. Kravchenko, S. I. Serednyakov, Yu. I. Skovpen, E. P. Solodov, K. Yu. Todyshev, A. J. Lankford, B. Dey, J. W. Gary, O. Long, A. M. Eisner, W. S. Lockman, W. Panduro Vazquez, D. S. Chao, C. H. Cheng, B. Echenard, K. T. Flood, D. G. Hitlin, Y. Li, D. X. Lin, S. Middleton, T. S. Miyashita, P. Ongmongkolkul, J. Oyang, F. C. Porter, M. Röhrken, B. T. Meadows, M. D. Sokoloff, J. G. Smith, S. R. Wagner, D. Bernard, M. Verderi, D. Bettoni, C. Bozzi, R. Calabrese, G. Cibinetto, E. Fioravanti, I. Garzia, E. Luppi, V. Santoro, A. Calcaterra, R. de Sangro, G. Finocchiaro, S. Martellotti, P. Patteri, I. M. Peruzzi, M. Piccolo, M. Rotondo, A. Zallo, S. Passaggio, C. Patrignani, B. J. Shuve, H. M. Lacker, B. Bhuyan, U. Mallik, C. Chen, J. Cochran, S. Prell, A. V. Gritsan, N. Arnaud, M. Davier, F. Le Diberder, A. M. Lutz, G. Wormser, D. J. Lange, D. M. Wright, J. P. Coleman, D. E. Hutchcroft, D. J. Payne, C. Touramanis, A. J. Bevan, F. Di Lodovico, G. Cowan, Sw. Banerjee, D. N. Brown, C. L. Davis, A. G. Denig, W. Gradl, K. Griessinger, A. Hafner, K. R. Schubert, R. J. Barlow, G. D. Lafferty, R. Cenci, A. Jawahery, D. A. Roberts, R. Cowan, S. H. Robertson, R. M. Seddon, N. Neri, F. Palombo, L. Cremaldi, R. Godang, D. J. Summers,[*] G. De Nardo, C. Sciacca, C. P. Jessop, J. M. LoSecco, K. Honscheid, A. Gaz, M. Margoni, G. Simi, F. Simonetto, R. Stroili, S. Akar, E. Ben-Haim, M. Bomben, G. R. Bonneaud, G. Calderini, J. Chauveau, G. Marchiori, J. Ocariz, M. Biasini, E. Manoni, A. Rossi, G. Batignani, S. Bettarini, M. Carpinelli, G. Casarosa, M. Chrzaszcz, F. Forti, M. A. Giorgi, A. Lusiani, B. Oberhof, E. Paoloni, M. Rama, G. Rizzo, J. J. Walsh, L. Zani, A. J. S. Smith, F. Anulli, R. Faccini, F. Ferrarotto, F. Ferroni, A. Pilloni, C. Bünger, S. Dittrich, O. Grünberg, T. Leddig, C. Voß, R. Waldi, T. Adye, F. F. Wilson, S. Emery, G. Vasseur, D. Aston, C. Cartaro, M. R. Convery, W. Dunwoodie, M. Ebert, R. C. Field, B. G. Fulsom, M. T. Graham, C. Hast, P. Kim, S. Luitz, D. B. MacFarlane, D. R. Muller, H. Neal, B. N. Ratcliff, A. Roodman, M. K. Sullivan, J. Va'vra, W. J. Wisniewski, M. V. Purohit, J. R. Wilson, S. J. Sekula, H. Ahmed, N. Tasneem, M. Bellis, P. R. Burchat, E. M. T. Puccio, J. A. Ernst, R. Gorodeisky, N. Guttman, D. R. Peimer, A. Soffer, S. M. Spanier, J. L. Ritchie, J. M. Izen, X. C. Lou, F. Bianchi, F. De Mori, A. Filippi, L. Lanceri, L. Vitale, F. Martinez-Vidal, A. Oyanguren, J. Albert, A. Beaulieu, F. U. Bernlochner, G. J. King, R. Kowalewski, T. Lueck, C. Miller, I. M. Nugent, J. M. Roney, R. J. Sobie, T. J. Gershon, P. F. Harrison, T. E. Latham, and S. L. Wu

(The *BABAR* Collaboration)

(Received 1 February 2023; accepted 23 March 2023; published 3 May 2023)

A new mechanism has been proposed to simultaneously explain the presence of dark matter and the matter-antimatter asymmetry in the Universe. This scenario predicts exotic B-meson decays into a baryon and a dark-sector antibaryon (ψ_D) with branching fractions accessible at B factories. We present a search for $B \to \Lambda\psi_D$ decays using data collected by the *BABAR* experiment at SLAC. This reaction is identified by fully reconstructing the accompanying B meson and requiring the presence of a single Λ baryon in the remaining particles. No significant signal is observed, and bounds on the $B \to \Lambda\psi_D$ branching fraction are derived in the range $0.13–5.2 \times 10^{-5}$ for $1.0 < m_{\psi_D} < 4.2$ GeV$/c^2$. These results set strong constraints on the parameter space allowed by the theory.

DOI: 10.1103/PhysRevD.107.092001

The nature of dark matter (DM) and the baryon asymmetry of the Universe (BAU) are perhaps two of the deepest mysteries of modern particle physics. The latest cosmological observations reveal that visible matter only accounts for about 15% of the matter in the Universe, while the remaining 85% is constituted by DM [1,2]. Beyond its coupling to gravity, the particle properties of DM remain to be elucidated, and many models have been proposed to explain the observed abundance. The visible matter density

[*] Deceased.

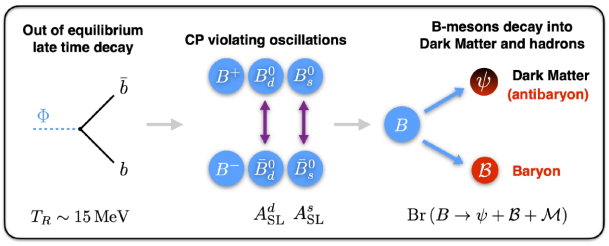

FIG. 1. Illustration of the B-mesogenesis mechanism. Figure taken from Ref. [6].

is equally mysterious, as cosmology predicts a universe born with equal amounts of matter and antimatter. A dynamical mechanism, baryogenesis, is required to produce an initial excess of baryons over antibaryons consistent with cosmic microwave background and big bang nucleosynthesis measurements [3,4].

The B-mesogenesis scenario has been recently proposed [5,6] to simultaneously explain the DM abundance and the BAU. This model introduces several new fields, including a light dark-sector antibaryon and a new TeV-scale color-triplet bosonic mediator. The baryogenesis mechanism relies on the out-of-thermal-equilibrium production of b and $\bar{b}$ quarks in the early Universe through the decay of a massive, long-lived scalar field Φ, as illustrated in Fig. 1. A fraction of these quarks hadronize into B^0 and $\bar{B}^0$ mesons, which undergo CP-violating oscillations before decaying into a baryon $\mathcal{B}$, a dark-sector antibaryon ψ_D, and any number of additional light mesons $\mathcal{M}$. As a result, matter-antimatter asymmetries are generated in the visible and dark sectors with equal but opposite magnitudes, keeping the total baryon number conserved.

We note that our search is strongly related in its experimental signature to a recently proposed [7] search for supersymmetry in B-meson decay to a baryon and undetected light neutralino.

The baryon asymmetry is determined by the charge asymmetry in semileptonic B decays, which specifies the level of CP violation in mixing in the B^0-$\bar{B}^0$ system, and the branching fraction of the inclusive $B \to \psi_D \mathcal{B}\mathcal{M}$ decays. The B-mesogenesis mechanism would imply a robust lower bound on the total branching fraction $\mathrm{BR}(B \to \psi_D \mathcal{B}M) > 10^{-4}$ [6]. Constraints on exclusive $B^0 \to \psi_D \mathcal{B}$ decays are calculated using phase-space considerations for different baryons [6]. The results depend on the effective operators $\mathcal{O}_{i,j} = \psi_D bij$ mediating the decay, where $i = u$, c and $j = d$, s specify the quark content. The ratio of exclusive to inclusive branching fractions ranges from about 1% to 100%, depending on the ψ_D mass. Furthermore, bounds on inclusive b decays with missing energy [8], searches for TeV-scale color-triplet scalars at the LHC [9,10], and dark matter stability require $0.94 < m_{\psi_D} < 3.5\,\mathrm{GeV}/c^2$ [6]. At present, the best constraints on this scenario arise from a measurement of the exclusive $B \to \psi_D \Lambda$ decay by the Belle Collaboration [11] excluding branching fractions larger than $\sim(2\text{–}3) \times 10^{-5}$ for $m_{\psi_D} > 1.0\ \mathrm{GeV}/c^2$.

We report herein a search for the decay $B^0 \to \psi_D \Lambda$ in the mass range $1.0 < m_{\psi_D} < 4.2\ \mathrm{GeV}/c^2$. The analysis is based on $398.5\ \mathrm{fb}^{-1}$ of data collected at the $\Upsilon(4S)$ resonance with the *BABAR* detector at the PEP-II e^+e^- storage ring at SLAC, corresponding to 4.35×10^8 $B\bar{B}$ pairs [12]. The *BABAR* detector is described in detail elsewhere [13,14]. An additional $32.5\ \mathrm{fb}^{-1}$ of data are used to optimize the analysis strategy and are subsequently discarded. The remaining data are not examined until the analysis procedure is finalized.

Simulated signal events are created using the EvtGen [15] Monte Carlo (MC) event generator. Eight different samples, each with a different ψ_D mass, are generated. The mass values range from 1 to $4.2\ \mathrm{GeV}/c^2$. The background is studied with samples of inclusive $e^+e^- \to B\bar{B}$ decays (EvtGen) and continuum $e^+e^- \to q\bar{q}$ events with $q = u$, d, s, c (JetSet [16]). The detector response is simulated with GEANT4 [17,18].

Since dark-sector particles escape undetected, we identify the signal by fully reconstructing the second B meson (B_{tag}) from hadronic decay modes, and we require the presence of a single Λ baryon among the remaining particles. The ψ_D is identified as the system recoiling against the B_{tag} and Λ candidates. Hadronic B-meson decays proceed mostly through charmed mesons, and the B_{tag} candidate is reconstructed via the decays $B \to SX$ by a hierarchical algorithm that combines a "seed" meson S, such as $D^{(*)0}$, $D^{(*)\pm}$, $D_s^{*\pm}$, or J/ψ, with a hadronic system X containing up to five kaons and/or pions with total charge 0 or ± 1 [19]. The selection of B_{tag} candidates is based on two kinematic variables: the energy difference $\Delta E = E_{\mathrm{beam}} - E_{\mathrm{tag}}$ and the beam-energy-substituted mass $m_{\mathrm{ES}}c^2 = \sqrt{E_{\mathrm{beam}}^2 - p_{B_{\mathrm{tag}}}^2 c^2}$, where E_{tag} and $p_{B_{\mathrm{tag}}}$ are the energy and momentum of the B_{tag} candidate in the e^+e^- center-of-mass frame, and E_{beam} is the beam energy in the same frame. ΔE and m_{ES} have to satisfy $|\Delta E| < 0.12$ GeV and $m_{\mathrm{ES}} > 5.20\ \mathrm{GeV}/c^2$, respectively. If more than one B_{tag} candidate is present in an event, the best one is chosen following these requirements: the highest B-decay-mode purity, defined as the fraction of correctly reconstructed B_{tag} candidates for a given decay mode, is selected, and the lowest value of $|\Delta E|$ is picked if there are several candidates having the same purity [20].

The remaining particles are associated with the signal $B \to \Lambda\psi_D$ candidate (B_{sig}). The Λ candidates are reconstructed as a pair of oppositely charged tracks identified as a proton and a pion. A kinematic fit is performed on the Λ candidate, constraining the two tracks to originate from the same point in space and requiring the momentum vector to point back to the beam interaction region. The Λ flight length is calculated as the distance between the primary

interaction point and the secondary decay vertex. The flight length significance, defined as the flight length divided by its uncertainty, must be greater than 1.0. If more than one combination of Λ candidates is found, the one with the smallest χ^2 from the kinematic fit is selected. After reconstructing the $B_{\rm tag}$ and Λ candidates, no additional track must be present in the event. The distributions of $m_{\rm ES}$ and the reconstructed Λ mass (m_Λ) are shown in Fig. 2. We require events to satisfy $5.27 < m_{\rm ES} < 5.29$ GeV$/c^2$ and $1.110 < m_\Lambda < 1.121$ GeV$/c^2$.

A multivariate selection using boosted decision trees (BDTs) [21] is used to further increase the signal purity. A BDT includes the following variables: the $m_{\rm ES}$ and ΔE of the $B_{\rm tag}$ candidate; information about the $B_{\rm tag}$ hadronic decay channel and its purity; the magnitude of the $B_{\rm tag}$ thrust vector, defined as the sum of the magnitudes of the momenta of all tracks and calorimeter clusters projected onto the thrust axis [20]; the $B_{\rm sig}$ momentum vector in the laboratory frame, inferred from the initial beam electrons and the recoiling $B_{\rm tag}$; the number of calorimeter clusters associated with $B_{\rm sig}$; the total neutral energy associated with $B_{\rm sig}$; the number of π^0 candidates associated with $B_{\rm sig}$; the Λ flight length significance; the χ^2 of the kinematic fit performed on the Λ candidate; and the energy and momentum of the Λ candidate in the laboratory frame. The ψ_D mass is specifically excluded from the BDT in order to limit potential bias in the classifier, and the BDT is trained on a signal sample spanning a wide range of ψ_D masses. The distribution of the BDT score, $\nu_{\rm BDT}$, is shown in Fig. 3. We select events with a BDT score greater than 0.75, selecting 41 events in the data. The resulting ψ_D mass distribution is shown in Fig. 4. Approximately half of the expected background consists of $e^+e^- \to q\bar{q}$ events, and the remainder arises from $B\bar{B}$ events.

The signal efficiency varies between 5.9×10^{-4} at $m_{\psi_D} = 1.0$ GeV$/c^2$ and 2.1×10^{-4} around $m_{\psi_D} = 4.2$ GeV$/c^2$, taking into account the $B_{\rm tag}$ reconstruction efficiency, the selection criteria, and the $\Lambda \to p\pi^-$ branching fraction. As shown in Fig. 3, the inclusive background MC samples do not accurately reproduce the data. This discrepancy from the $B\bar{B}$ component arises from a mismodeling of several branching fractions used in the simulation, resulting in differences in $B_{\rm tag}$ reconstruction efficiencies [22], as well as differences in charged and neutral particle reconstruction efficiencies, PID efficiencies, and the modeling of variables used in the BDT. We correct the simulation in a two-step procedure, using sideband data selected with the criteria described above, applied before the BDT selection, except with the looser

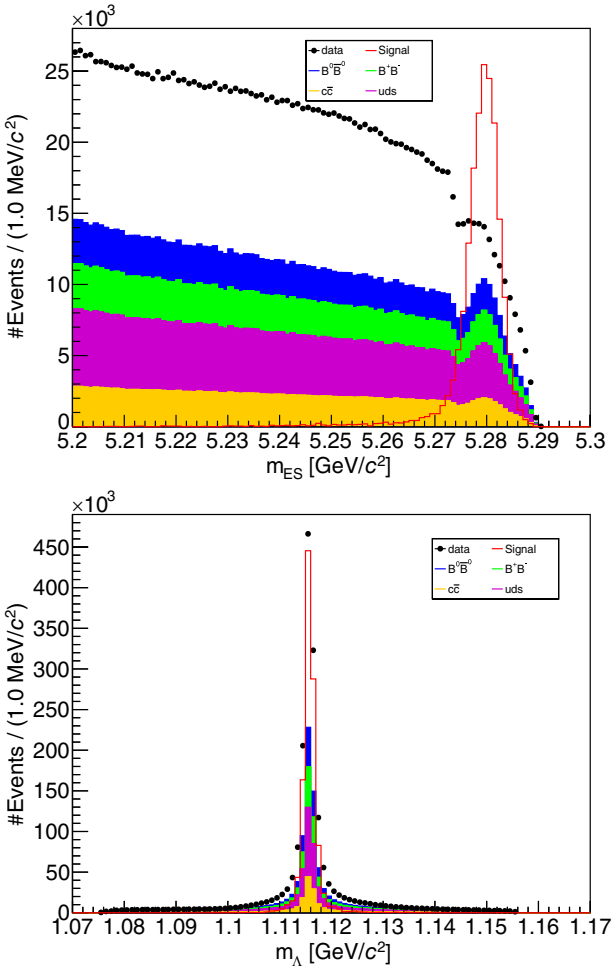

FIG. 2. Distributions of the energy-substituted mass, $m_{\rm ES}$ (top), and the reconstructed Λ mass, m_Λ (bottom), for data (points), signal MC for $m_{\psi_D} = 2.0$ GeV$/c^2$ (red histogram) and inclusive background MC predictions (stacked histograms, no corrections applied). The normalization of the signal events is arbitrary.

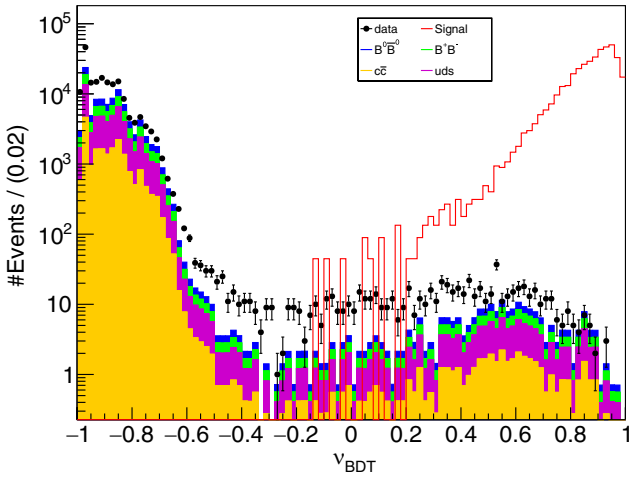

FIG. 3. The distribution of the BDT score after applying all other selection criteria for data (points), signal MC for $m_{\psi_D} = 2.0$ GeV$/c^2$ (red histogram), and inclusive background MC predictions (stacked histograms, no corrections applied). The normalization of the signal events is arbitrary.

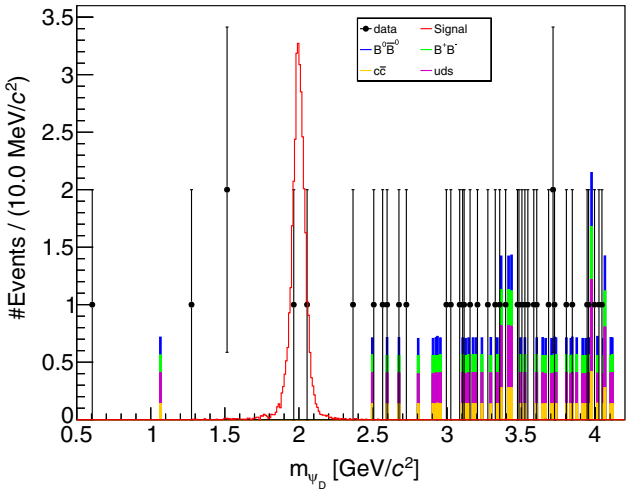

FIG. 4. The distribution of the ψ_D mass (m_{ψ_D}) after applying all selection criteria for data (points), signal MC for $m_{\psi_D} = 2.0\ \mathrm{GeV}/c^2$ (red histogram), and inclusive background MC predictions (stacked histograms). The normalization of the signal events is arbitrary.

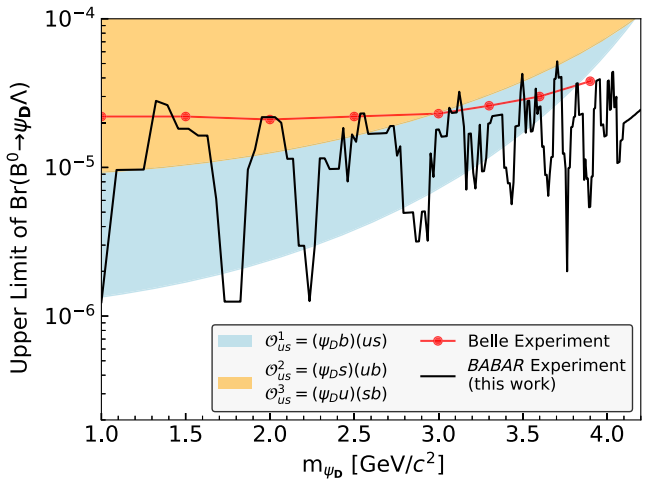

FIG. 5. Upper limits on the $B^0 \to \psi_D \Lambda$ branching fraction at a 90% CL, together with previous constraints [11]. The light blue and orange [orange-only] region shows the values of the $B^0 \to \psi_D \Lambda$ branching fraction allowed to successfully generate B mesogenesis for the $\mathcal{O}^1_{us} = (\psi_D b)(us)$ [$\mathcal{O}^2_{us} = (\psi_D s)(ub)$ and $\mathcal{O}^3_{us} = (\psi_D u)(sb)$] effective operators [6].

requirement $5.20 < m_{\mathrm{ES}} < 5.29\ \mathrm{GeV}/c^2$. The region $-0.5 < \nu_{\mathrm{BDT}} < 0.75$, largely dominated by $e^+e^- \to q\bar{q}$ ($q = u, d, s, c$) events, is used to extract a correction factor for continuum production, f_{udsc}, by rescaling the corresponding MC predictions to the number of observed events. The correction factor for $B\bar{B}$ production, $f_{B^0\bar{B}^0}$, is determined from data in the complementary region $\nu_{\mathrm{BDT}} < -0.5$, assuming equal contributions from $B^0\bar{B}^0$ and B^+B^-. We obtain $f_{udsc} = 1.34 \pm 0.10$ and $f_{B^0\bar{B}^0} = 1.06 \pm 0.08$. Under the assumption that the $B\bar{B}$ correction factor is independent of the signal B-decay mode, we rescale the signal efficiency by $f_{B^0\bar{B}^0}$ and propagate the corresponding uncertainty as a systematic uncertainty.

We extract the signal yield by scanning the ψ_D mass spectrum in steps of the signal mass resolution, σ_m, probing a total of 193 mass hypotheses. The resolution is estimated by performing fits of a Bukin function [23] to the ψ_D mass distribution for each signal MC sample, and interpolating the results to the full mass range. The results vary between 90 MeV/c^2 at $m_{\psi_D} = 1.0\ \mathrm{GeV}/c^2$ and 6 MeV/c^2 at $m_{\psi_D} = 4.2\ \mathrm{GeV}/c^2$. The signal yield is determined by counting the number of events in a window of $\pm 3\sigma_m$ centered around the ψ_D mass hypothesis. The background is evaluated with a Poisson counting approach in two sideband regions of $\pm 3\sigma_m$ surrounding the signal window in the data, except near $m_{\psi_D} = 4.2\ \mathrm{GeV}/c^2$, where a single region is used. The largest local significance is found to be 2.3σ, observed near $m_{\psi_D} = 3.7\ \mathrm{GeV}/c^2$, corresponding to a global significance of 0.4σ after including trial factors [24], consistent with the null hypothesis.

In the absence of a signal, upper limits on the branching fraction $B^0 \to \psi_D \Lambda$ are derived at a 90% confidence level (CL) by applying a profile likelihood method [25] for each ψ_D mass hypothesis. The number of signal and background events is assumed to follow Poisson distributions, while the efficiency is modeled with a Gaussian having a variance equal to the total systematic uncertainty. Systematic uncertainties arising from track and neutral reconstruction efficiencies, B_{tag} reconstruction efficiencies, selection criteria, and modeling of the BDT variables are included in the $B\bar{B}$ correction factor described above. Other sources of uncertainty include the $\Lambda \to p\pi^-$ branching fraction (0.8%), the integrated luminosity (0.6%) [12], and the limited statistical precision of the signal MC samples (0.7%–4.6%). The total systematic uncertainty, obtained by summing in quadrature the different contributions, varies between 7.8% and 9.1%.

The results are displayed in Fig. 5, together with the previous measurement from the Belle Collaboration and theoretical predictions for different type of operators generating B mesogenesis. We probe branching fractions in the range $0.13\text{–}5.2 \times 10^{-5}$, improving previous constraints by up to an order of magnitude. These bounds exclude most of the remaining parameter space for the $\mathcal{O}^2_{us} = (\psi_D s)(ub)$ and $\mathcal{O}^3_{us} = (\psi_D u)(sb)$ operators, and a significant fraction of the region allowed for $\mathcal{O}^1_{us} = (\psi_D b)(us)$ operators above $m_{\psi_D} > 2.8\ \mathrm{GeV}/c^2$.

In summary, we report a search for baryogenesis and dark matter in the process $B^0 \to \Lambda\psi_D$ with a fully reconstructed B_{tag} meson. No significant signal is observed, and upper limits on the branching fraction at the level of $10^{-6}\text{–}10^{-5}$ are set. These results exclude a large fraction of the parameter space allowed by B mesogenesis. Future measurements at Belle-II should be able to fully explore the remaining region.

We thank G. Elor and M. Escudero for useful discussions on the B-mesogenesis mechanism. We are grateful for the extraordinary contributions of our PEP-II colleagues in achieving the excellent luminosity and machine conditions that have made this work possible. The success of this project also relies critically on the expertise and dedication of the computing organizations that support *BABAR*. The collaborating institutions wish to thank SLAC for its support and the kind hospitality extended to them.

[1] P. A. R. Ade *et al.* (Planck Collaboration), Astron. Astrophys. **594**, A13 (2016).
[2] N. Aghanim *et al.* (Planck Collaboration), Astron. Astrophys. **641**, A6 (2020).
[3] M. Tanabashi *et al.* (Particle Data Group), Phys. Rev. D **98**, 030001 (2018).
[4] R. H. Cyburt, B. D. Fields, K. A. Olive, and T.-H. Yeh, Rev. Mod. Phys. **88**, 015004 (2016).
[5] G. Elor, M. Escudero, and A. E. Nelson, Phys. Rev. D **99**, 035031 (2019).
[6] G. Alonso-Álvarez, G. Elor, and M. Escudero, Phys. Rev. D **104**, 035028 (2021).
[7] C. O. Dib, J. C. Helo, V. E. Lyubovitskij, N. A. Neill, A. Soffer, and Z. S. Wang, J. High Energy Phys. 02 (2023) 224.
[8] R. Barate *et al.* (ALEPH Collaboration), Eur. Phys. J. C **19**, 213 (2001).
[9] A. M. Sirunyan *et al.* (CMS Collaboration), J. High Energy Phys. 10 (2019) 244.
[10] G. Aad *et al.* (ATLAS Collaboration), J. High Energy Phys. 02 (2021) 143.
[11] C. Hadjivasiliou *et al.* (Belle Collaboration), Phys. Rev. D **105**, L051101 (2022).
[12] J. P. Lees *et al.* (*BABAR* Collaboration), Nucl. Instrum. Methods Phys. Res., Sect. A **726**, 203 (2013).
[13] B. Aubert *et al.* (*BABAR* Collaboration), Nucl. Instrum. Methods Phys. Res., Sect. A **479**, 1 (2002).
[14] B. Aubert *et al.* (*BABAR* Collaboration), Nucl. Instrum. Methods Phys. Res., Sect. A **729**, 615 (2013).
[15] D. J. Lange, Nucl. Instrum. Methods Phys. Res., Sect. A **462**, 152 (2001).
[16] T. Sjöstrand, S. Mrenna, and P. Skands, J. High Energy Phys. 05 (2006) 026.
[17] S. Agostinelli *et al.* (GEANT4 Collaboration), Nucl. Instrum. Methods Phys. Res., Sect. A **506**, 250 (2003).
[18] J. Allison *et al.*, IEEE Trans. Nucl. Sci. **53**, 270 (2006).
[19] J. P. Lees *et al.* (*BABAR* Collaboration), Phys. Rev. D **100**, 111101 (2019).
[20] A. J. Bevan *et al.*, Eur. Phys. J. C **74**, 3026 (2014).
[21] Y. Freund and R. E. Schapire, J. Comput. Syst. Sci. **55**, 119 (1997).
[22] B. Aubert *et al.* (*BABAR* Collaboration), Phys. Rev. D **80**, 111105 (2009).
[23] A. Bukin, arXiv:0711.4449.
[24] E. Gross and O. Vitells, Eur. Phys. J. C **70**, 525 (2010).
[25] W. A. Rolke, Angel M. López, and Jan Conrad, Nucl. Instrum. Methods Phys. Res., Sect. A **551**, 493 (2005).